Available online at www.sciencedirect.com
ScienceDirect
Trans. Nonferrous Met. Soc. China 34(2024) 4063−4074
Transactions of Nonferrous Metals Society of China
www.tnmsc.cn

Intensifying recovery of metallic aluminum in secondary aluminum dross by alkali roasting−water leaching

Chen LI, Wei LIU, Fen JIAO, Liang-min DONG, Shi-yang LIU, Wen-qing QIN

School of Minerals Processing and Bioengineering, Central South University, Changsha 410083, China

Received 7 May 2023; accepted 20 December 2023

Abstract: An innovative process was proposed to recover metallic aluminum from secondary aluminum dross (SAD) by alkali roasting−water leaching. Thermodynamic calculations and experimental results were used to illustrate the phase transformation and reaction mechanism of the alkali roasting process. The leaching behaviors of roasted residue were also analyzed. Under optimal conditions, the aluminum extraction rate reached 93.08%. In addition, the kinetics of the water leaching of roasted products was studied through shrinking core model, and it was revealed that the leaching process of aluminum was in accord with diffusion control. The apparent activation energy of the leaching process was calculated to be 3.44 kJ/mol. Based on the above study, the underlying mechanism of the alkali roasting−water leaching was clarified.

Key words: secondary aluminum dross; aluminum recovery; selective separation; alkali roasting; water leaching

1 Introduction

Aluminum, a metal with the second largest output, got its world-wide gross production of 67.243×10^6 t in 2021, which was much higher than other nonferrous metals [1−3]. However, a large amount of aluminum dross can be formed when the molten aluminum contacts with air and gets oxidized through the aluminum electrolysis, processing and regeneration [4]. The amount of secondary aluminum dross (SAD) generated in the recycling process of recycled aluminum is 10−20 times that of primary aluminum dross (PAD) obtained from traditional electrolysis [5,6]. For 1 t of molten aluminum, 1.5%−2.5% of PAD and 8%−15% of SAD can be produced, respectively [7−9]. The composition of SAD is largely up to the production process of recycled aluminum and it mainly contains metallic aluminum, aluminum oxide, aluminum nitride, aluminum carbide, silicon dioxide, heavy metals and salts [10−12]. The complex composition means that SAD is inappropriate for direct reuse by conventional methods. Therefore, over 70% of SAD is still currently treated by landfill which not only wastes its valuable resources but also leads to potential environmental pollution [13−15].

Aluminum is the most valuable element in the recycling of SAD, so an environmentally-friendly and efficient extraction of aluminum is essential to realize the utilization of aluminum dross. Up to now, hydrometallurgical process and pyrometallurgical process have been reported to be routines for SAD. The hydrometallurgical process, which is of low energy consumption and suitable for aluminum dross with low content of aluminum, can be categorized into alkali leaching and acid leaching [16−20]. Alkali leaching and acid leaching usually use solutions such as sodium hydroxide, sulfuric acid, and hydrochloric acid of certain concentration to selectively leach aluminum from

Corresponding author: Wei LIU, Tel: +86-13787007421, E-mail: liuweipp1@126.com
DOI: 10.1016/S1003-6326(24)66658-6

aluminum dross. However, hydrometallurgical process suffers from potential atmospheric pollution (H_2, CH_4 and NH_3) which may caused by metallic aluminum, aluminum carbide and aluminum nitride in the aluminum dross through hydrolysis reactions. In addition, the presence of α-Al_2O_3 and $MgAl_2O_4$ which are insoluble in acid and alkali solutions, also makes it difficult to achieve a high recovery rate of aluminum in leaching [21−23].

The pyrometallurgical process, characterized by its short process and high efficiency, can be divided into comprehensive utilization and aluminum recovery. Comprehensive utilization commonly applies SAD as an addition and combines it with other raw materials such as clay, kaolin, and rutile to manufacture construction materials, firebrick or ceramics products, but the added value and economic benefits are quite limited [24−27]. Recovering process mainly includes reduction smelting and alkali roasting−leaching. Reduction smelting is to obtain metallic aluminum products at smelting temperatures (>1600 °C) with silicon and carbon as reducing agents, but it is not recommended for large-scale application due to the high energy consumption in high-temperature treatment [28−30]. The alkali roasting−leaching process has been widely utilized for extracting valuable metals from complex materials. The alkali roasting of aluminum-containing materials involves converting insoluble Al_2O_3 or $MgAl_2O_4$ into water-soluble $NaAlO_2$, and separating aluminum from other elements through alkali leaching or water leaching. Compared with leaching and smelting methods, this process achieves a high recovery rate at low cost with no discharge of harmful gases, thus it can be regarded as a practical and feasible process [31−34].

In SAD, the surface of the metallic aluminum is covered with a dense oxidation layer. Therefore, for the recycling of metallic aluminum, it is of great significance to break this oxidation layer and generate sodium aluminate [35,36]. In this paper, a facile process of the alkali roasting−water leaching was adopted to selectively extract aluminum from SAD. Firstly, the effects of temperature, dosage of NaOH and roasting time on the conversion rate of $NaAlO_2$ were studied. The phase transformation and reaction mechanism were clearly clarified. Then, the leaching behaviors of the roasted residue were investigated using thermodynamic and kinetic analysis, and the control conditions of leaching reaction were determined. Finally, a new process for the utilization of SAD was established and some theoretical guidance for the recovery of SAD was also provided.

2 Experimental

2.1 Starting materials

The SAD used in this study was from a aluminum plant in Hunan province, China. The chemical compositions of the samples were presented in Table 1, which mainly contained elements such as Al, Fe, Ca and Si. As shown in Table 2, the phase compositions of aluminum in the SAD were mainly Al_2O_3 and Al. XRD was adopted to identify the mineral phases in the SAD and the results were displayed in Fig. 1(a). The SEM micrograph of the SAD sample and the corresponding EDS analysis results were shown in Fig. 1(b) and Table 3, respectively. As presented in Fig. 1(b) and Table 3, the particle size of SAD was fine and the surface of metallic aluminum was covered with a dense oxidation layer.

Table 1 Main compositions of SAD (wt.%)

Al	Fe	Ca	Si	K	Cl	S	O
52.78	1.04	3.73	1.55	1.66	2.33	0.11	34.86

Table 2 Content of aluminum phase in SAD (wt.%)

Total Al	Al_2O_3	Metallic Al	AlN
52.78	23.37	29.17	0.24

Table 3 EDS results of SAD sample

Point No. in Fig. 1(b)	Content/wt.%				
	Al	O	N	Si	Fe
1	45.6	35.1	14.5		
2	95.1	4.9			
3	43.7			24.3	29.9
4	48.8	50.9			
5	94.3	5.7			

2.2 Principles of experimental procedure

Figure 2 shows the schematic diagram of the alkali roasting−water leaching experiment device. The experimental procedure was as follows. The samples were dried at 105 °C for 24 h by a drying

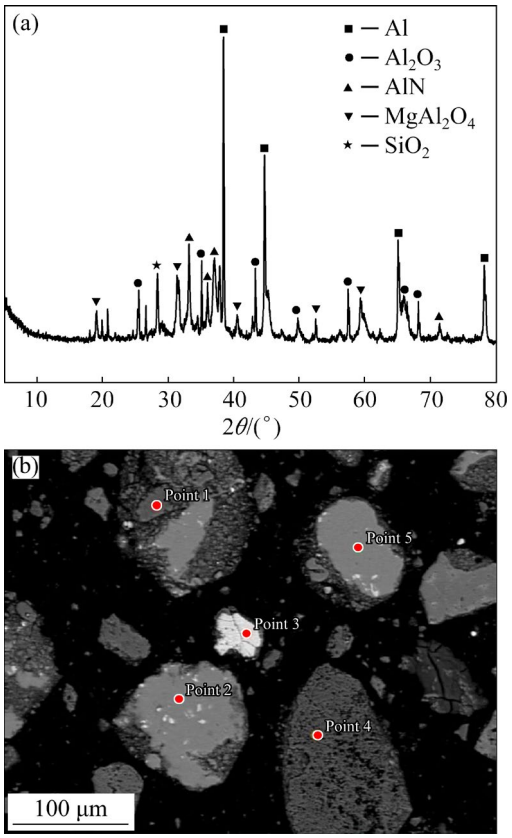

Fig. 1 XRD pattern (a) and SEM micrograph (b) of SAD sample

oven and then 30 g SAD and different dosages of NaOH were thoroughly mixed by a mortar and pestle. The mixed materials were put into a ceramic crucible, placed in a muffle furnace (SXL1008, maximum temperature of 1200 °C and accuracy of ±20 °C), and heated at required temperature and roasted under the atmosphere of air. After roasting and further cooling, the samples were taken out and then crushed by a vibrating disc mill machine for analysis and subsequent experiments. XRD and ICP methods were used to analyze and identify the chemical compositions of the roasted residues. The conversion rate of $NaAlO_2$ was calculated as follows:

$$\alpha_{\mathrm{Al-NaAlO_2}}=\frac{m_{\mathrm{residue}}\cdot w_{\mathrm{Al-NaAlO_2}}}{m_{\mathrm{residue}}\cdot w_{\mathrm{Al}}}\times 100\% \quad (1)$$

where $\alpha_{\mathrm{Al-NaAlO_2}}$ is the conversion rate of $NaAlO_2$ from the Al (%); $w_{\mathrm{Al-NaAlO_2}}$ is mass fraction of Al in the $NaAlO_2$ (%); w_{Al} is mass fraction of Al in the roasted residue (%); m_{residue} is the mass of the roasted residue (g).

Under optimal roasting conditions, a series of leaching tests were performed in a water bath equipment and the samples were heated at a fixed test temperature to investigate the water solubility of alkali roasted slag. ICP was used to determine the concentration of aluminum and the leaching rate of aluminum. The leaching rate of aluminum was calculated as

$$\alpha_{\mathrm{Al}}=\frac{\rho_{\mathrm{Al}}\cdot V}{m_{\mathrm{residue}}\cdot w_{\mathrm{Al}}}\times 100\% \quad (2)$$

where α_{Al} is the leaching rate of the total Al (%); ρ_{Al} is the total concentration of Al in the leaching (g/L); V is the leachate volume (L).

3 Results and discussion

3.1 Thermodynamic analysis

In order to identify the complicated alkali roasting process, possible reactions were listed in Reactions (3)−(14). The standard Gibbs free energy changes in these reactions in the temperature range

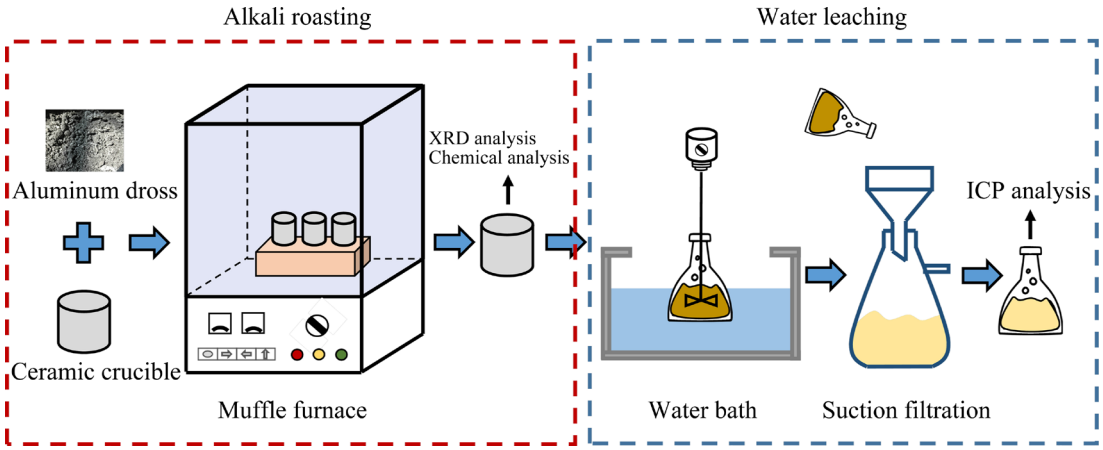

Fig. 2 Schematic diagram of alkali roasting−water leaching process

of 200−1000 °C were shown in Fig. 3.

$$4Al+4NaOH+3O_2=4NaAlO_2+2H_2O \quad (3)$$

$$Al_2O_3+2NaOH=2NaAlO_2+H_2O \quad (4)$$

$$4AlN+4NaOH+3O_2=4NaAlO_2+2H_2O+2N_2\uparrow \quad (5)$$

$$Al_4C_3+4NaOH+6O_2=4NaAlO_2+3CO_2+2H_2O \quad (6)$$

$$Al_2O_3+CaO=CaAl_2O_4 \quad (7)$$

$$Al_2O_3+MgO=MgAl_2O_4 \quad (8)$$

$$CaAl_2O_4+2NaOH=CaO+2NaAlO_2+H_2O \quad (9)$$

$$MgAl_2O_4+2NaOH=MgO+2NaAlO_2+H_2O \quad (10)$$

$$SiO_2+2NaOH=Na_2SiO_3+H_2O \quad (11)$$

$$NaAlO_2+SiO_2=NaAlSiO_4 \quad (12)$$

$$NaAlO_2+2CaSiO_3=NaAlSiO_4+Ca_2SiO_4 \quad (13)$$

$$NaAlO_2+2MgSiO_3=NaAlSiO_4+Mg_2SiO_4 \quad (14)$$

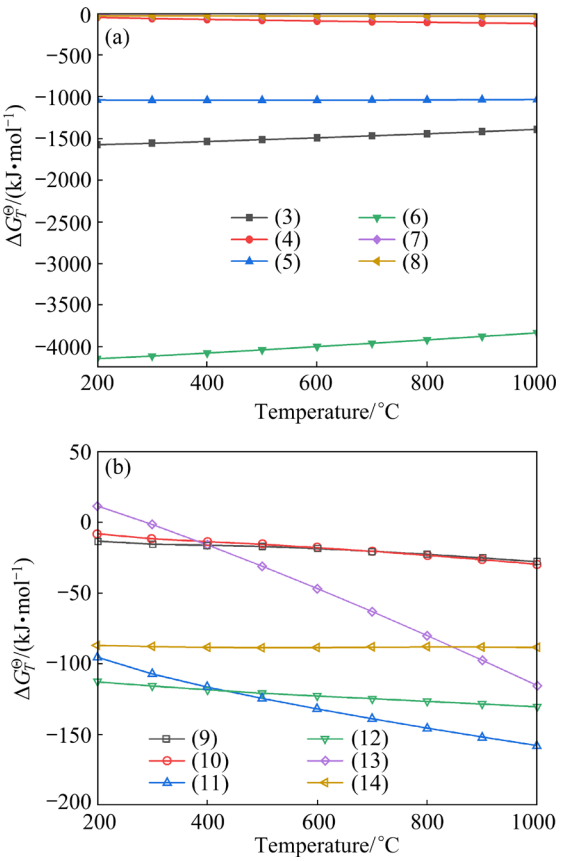

Fig. 3 $\Delta G_T^{\Theta}-T$ diagrams of Reactions (3)−(14) at different temperatures

As displayed in Fig. 3, main reactions occurred in the range of roasting temperatures. Here, Al, AlN, and Al_4C_3 positively reacted with oxygen and NaOH to form $NaAlO_2$ and release N_2 and H_2O in the alkali roasting process. The Gibbs free energy changes (ΔG) for reactions between NaOH, $CaAl_2O_4$ and $MgAl_2O_4$ were negative, showing that aluminates could be decomposed through alkali roasting. In addition, NaOH could react with SiO_2 to produce water- soluble sodium silicate, probably resulting in a loss of alkali.

The equilibrium compositions of the reaction products were calculated by the Equilibrium compositions module of HSC 9.0 and shown in Fig. 4. As presented in Fig. 4(a), with increasing amount of O_2 during the alkali roasting process, the amount of Al gradually declined while $NaAlO_2$ gradually increased, which indicated that O_2 was necessary for the reaction between Al and NaOH. It can be seen from Fig. 4(b) that Al_2O_3 gradually reacted and transformed into $NaAlO_2$ with the increase in the amount of NaOH, whereas it also led to the production of $NaAlSiO_4$. Under the fixed condition of 1 kmol SiO_2, the content of $NaAlSiO_4$ first increased apparently and then decreased with the addition of NaOH, indicating that excessive NaOH could hindered the generation of $NaAlSiO_4$ in the system.

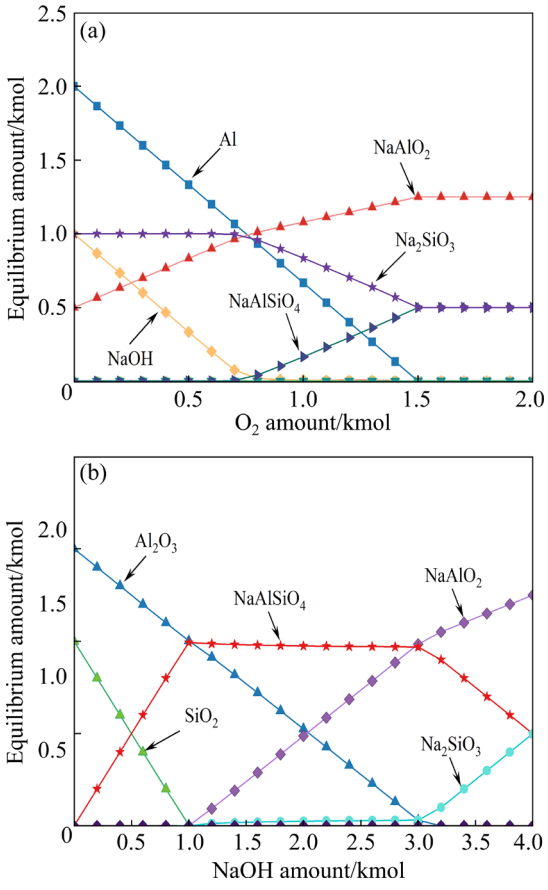

Fig. 4 Equilibrium phase diagrams of alkali roasting with different O_2 (a) and NaOH (b) amounts

3.2 Alkali roasting behavior of aluminum

To specifically explore the transformation of aluminum into $NaAlO_2$ during the alkali roasting process, the effects of different factors, i.e., the dosage of sodium hydroxide (NaOH/SAD mass ratio), reaction temperature and holding time were investigated. Figure 5 presents the effect of dosage of sodium hydroxide on the alkali roasting behavior of aluminum in the dross. According to Fig. 5(a), the conversion rate of $NaAlO_2$ increased significantly with the increasing from 0.25 to 1.0 and then became stable. It was worth noting that the conversion rate of $NaAlO_2$ increased slowly and gradually from 90.78% to 92.67% with the NaOH/SAD mass ratio changing from 1.0 to 1.5. Thus, we could conclude that excessive addition of NaOH had little effect on the transformation of $NaAlO_2$. In order to elucidate the reason for the phenomenon that the conversion of $NaAlO_2$ changed with the addition of NaOH, the roasting residues at different NaOH/SAD mass ratios were analyzed by XRD. From Fig. 5(b), it could be seen that the main diffraction peak at NaOH/SAD mass ratio of 0.25 was $NaAlO_2$ and Al and the peak of Al_2O_3 thoroughly disappeared at this point, thus indicating that Al_2O_3 reacted preferentially with NaOH to form $NaAlO_2$. The NaOH peak appeared when the NaOH/SAD mass ratio was 0.75. NaOH at this point was evidently in excess while the peak of Al still obviously existed. When the amount of NaOH continuously increased, the peak of Al gradually weakened till it completely disappeared. The potential reason for this was that the increase of NaOH amount provided a greater oxygen potential for the roasting system and considerably promoted the oxidation of metallic aluminum [34,37].

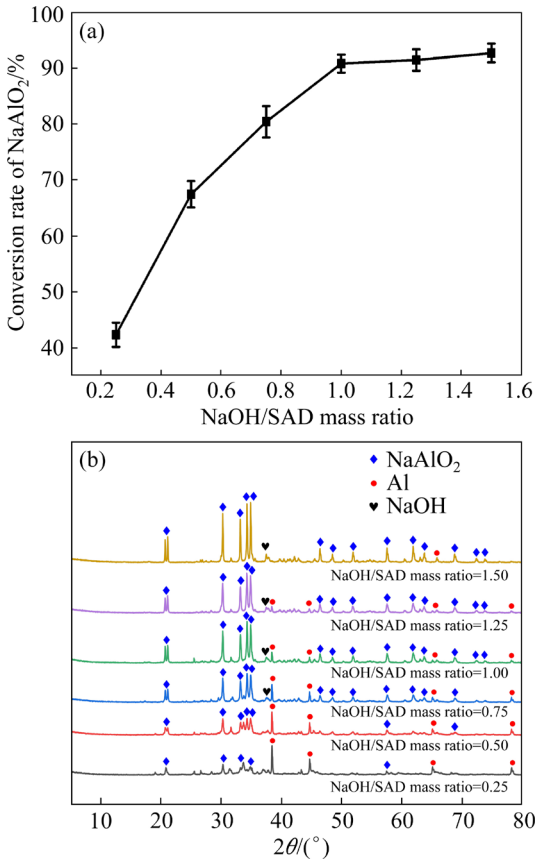

Fig. 5 Effect of NaOH dosage (NaOH/SAD mass ratio) on conversion rate of $NaAlO_2$ (a) and XRD patterns of roasted residues (b)

Given that temperature is an important thermodynamic factor in chemical reaction, the influence of roasting temperature on the conversion rate of $NaAlO_2$ is shown in Fig. 6. In Fig. 6(a), the conversion rate of $NaAlO_2$ increased from 63.54% to 90.78% when the roasting temperature rose from 400 to 800 °C, indicating that the increase of temperature could benefit the reaction of aluminiferous phase with NaOH. The XRD patterns of roasted residues obtained at different roasting temperatures are shown in Fig. 6(b). It could be seen that the diffraction peaks of $NaAlO_2$ were gradually strengthened while those of Al were weakened with the increase of roasting temperature. Thus, the conclusion could be drawn that certain temperature was essential for the formation of $NaAlO_2$ and low roasting temperature was not conducive to the transformation of Al to $NaAlO_2$. It was worth noting that the diffraction peaks of $MgAlO_2$ appeared when the roasting temperature was lower than 600 °C, because it was hard for the magnesia alumina spinel to react with sodium hydroxide at low temperatures [38]. As the temperature increased, the peak of $MgAlO_2$ gradually disappeared due to Reaction (10), which improves the conversion rate of aluminum. Therefore, it was of extreme significance to keep high temperature in the alkali roasting process. However, the roasting residue could be sintered when roasting temperature exceeded 800 °C and it would be hard for the residue to be ground.

The influence of roasting time on the conversion rate of $NaAlO_2$ was presented in Fig. 7(a). It could be found that when the roasting time increased from 0.5 to 1 h, the conversion rate increased from 80.78% to 90.78%. Further increase of the roasting time to 2 h would witness the decline

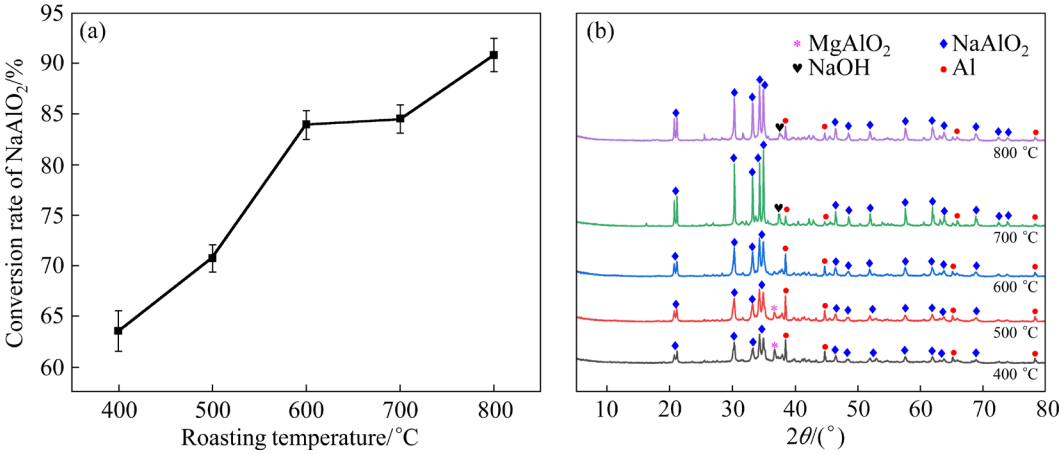

Fig. 6 Effect of roasting temperature on conversion rate of $NaAlO_2$ (a) and XRD patterns of roasted residues (b)

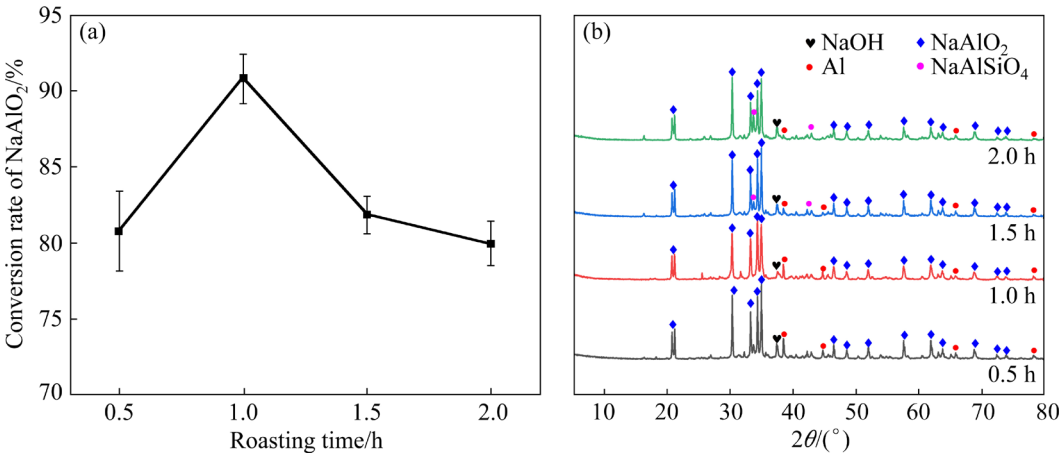

Fig. 7 Effect of roasting time on conversion rate of $NaAlO_2$ (a) and XRD patterns of roasted residues (b)

of the conversion rate to 79.96%. It was revealed that too long roasting time did not contribute to the increase in the conversion rate of $NaAlO_2$. To further illustrate the reason for the decline on the conversion rate of $NaAlO_2$, the phase compositions of roasted residues under different roasting time conditions analyzed by XRD were exhibited in Fig. 7(b). It was observed in Fig. 7(b) that the diffraction peaks of $NaAlO_2$ basically kept steady with the increase of roasting time, whereas the diffraction peaks of Al gradually disappeared. The potential explanation for this phenomenon was that the oxidation of Al to Al_2O_3 was the prerequisite condition for the reaction of Al_2O_3 with NaOH and the subsequent generation of $NaAlO_2$ during the alkali roasting process. However, a dense alumina layer could be formed after the oxidization on the surface of the Al, thus preventing the oxidation of the interior Al. Therefore, only after the complete reaction between the surface alumina layer and sodium hydroxide could the underlying metallic Al surfaces possibly conduct further reactions, which greatly limited and hindered the conversion of Al to $NaAlO_2$ [39−41]. When the reaction time was extended to 1.5 h, peaks of $NaAlSiO_4$ appeared in the roasted residue, indicating that too longer roasting time could promote the reactions between $NaAlO_2$ and silicate in the system and result in a loss of aluminum.

3.3 Water solubility of roasted slag

In order to study the water solubility of roasted residues, a water leaching experiment was conducted on the roasted residues under optimal roasting conditions. 90.78% aluminum could be transformed to $NaAlO_2$ under optimal roasting conditions, i.e., NaOH/SAD mass ratio of 1.0, temperature of 800 °C and roasting time of 60 min. To explore the dissolution behavior of alumina in water systems, the potential−pH (φ−pH) diagrams of the Al−H_2O system at 25 and 80 °C were drawn in Fig. 8(a) using Factsage8.0 software. According to Fig. 8(a),

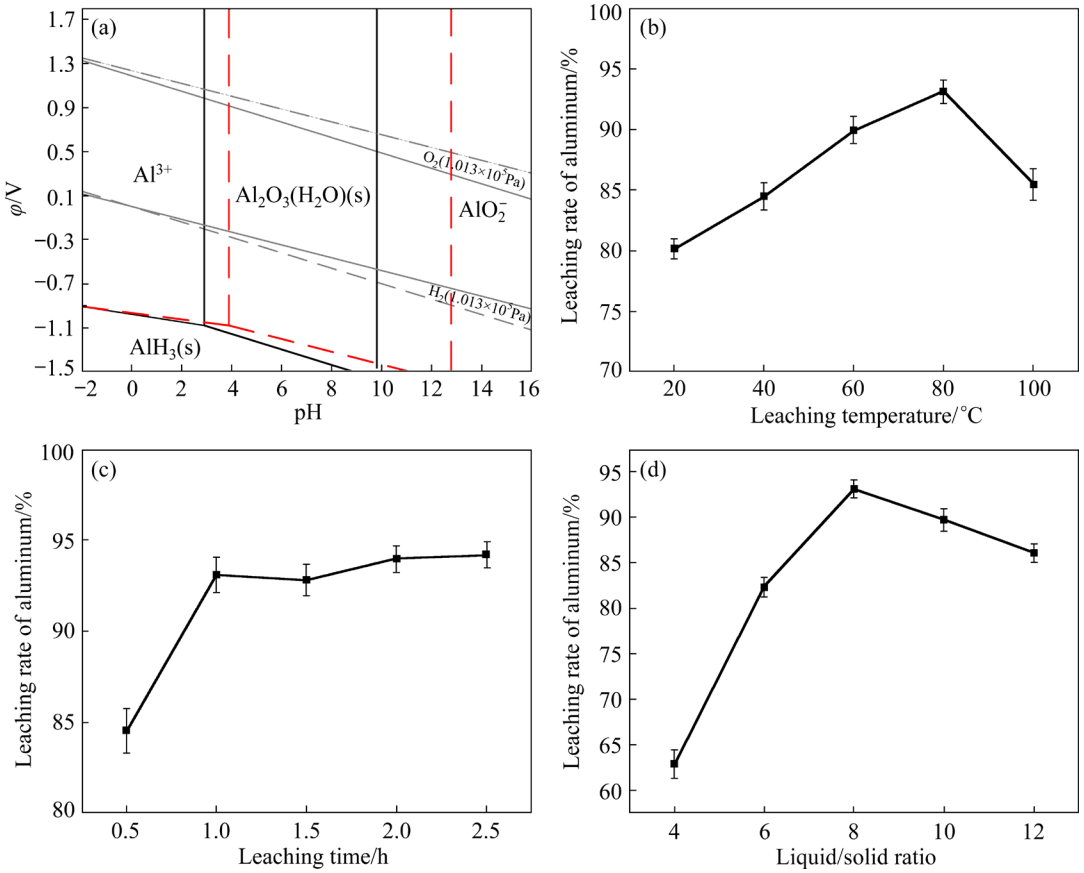

Fig. 8 φ−pH diagrams for Al−H_2O system at 25 °C (solid line) and 80 °C (dotted line) (a), and effects of leaching temperature (b), leaching time (c) and liquid/solid ratio (d) on leaching rate of aluminum

the pH of solution must be greater than 12 to dissolve Al_2O_3 when the system temperature was 25 °C. However, the required pH of solution turned 10 when the system temperature was increased to 80 °C, indicating that an increase in temperature was conducive to the dissolution of Al_2O_3 in alkaline solutions. After sodium aluminate dissolved in water as a weak base, the increase of the temperature was apparently conducive to the dissolution of the unreacted aluminum-containing substances such as metallic aluminum and alumina in the roasted residue [42−44].

Figure 8(b) presents the effect of leaching temperature on the leaching rate of aluminum, from which it can be found that the solubility of Al ascended at the beginning and then descended gradually with the leaching temperature rising from 20 to 80 °C and the leaching rate of aluminum reached its maximum value of 93.08% at 80 °C. The value was close to the conversion rate of sodium aluminate; therefore, it could be concluded that the other aluminum-containing phases in the material were difficult to dissolve in water except $NaAlO_2$. When the water leaching temperature reached 100 °C, the leaching rate significantly decreased, which might be attributed to the reactions of sodium aluminate with sodium silicate. The possible chemical equations were as follows:

$$2Na_2SiO_3+2NaAlO_2+2H_2O=Na_2Al_2Si_2O_8\downarrow+4NaOH \quad (15)$$

Figure 8(c) presents the effect of leaching time on the leaching rate of aluminum, from which it can be found that the leaching rate increased from 84.53% to 94.16% with the leaching time prolonging from 0.5 to 2.5 h. Possible explanation for this phenomenon was that the insoluble aluminum-containing phases in the roasting residue such as metallic aluminum gradually dissolved into the solution. Figure 8(d) presents the effect of liquid/solid ratio on the leaching rate of aluminum. The leaching rate gradually increased with the liquid/solid ratio changing from 4 to 8. However, with liquid/solid ratio exceeding 10, the leaching rate of aluminum began to decrease slightly. The reason might be that the increase in the liquid/solid

ratio led to the decline in the pH of the solution and resulted in the precipitation of $Al(OH)_3$, thus the loss of aluminum.

With the application of appropriate roasting parameters, the main compositions of the leaching residue were determined by the XRF and listed in Table 4. The contents of Al, Na, Ca and Si were 11.80, 19.44, 6.432 and 6.454 wt.%, respectively. The XRD pattern and SEM image in Fig. 9 indicate that the main phases in the residue were calcium carbonate and magnesium oxide. However, the aluminum-containing phases were more difficult to identify, and the leaching residue particles were irregular and extremely fine.

Table 4 Main compositions of leaching residue (wt.%)

Al	Na	Ca	Si	Fe	Mg	Ba	O
11.80	19.44	6.432	6.454	1.778	3.218	0.688	31.40

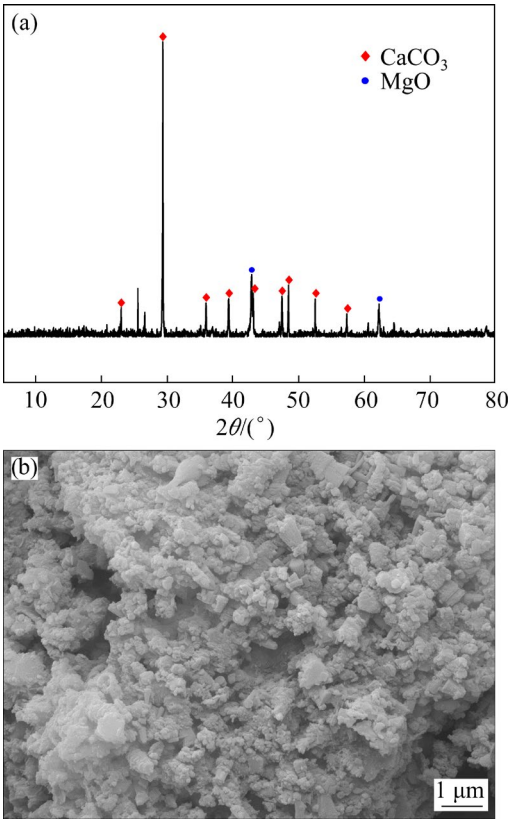

Fig. 9 XRD pattern (a) and SEM image (b) of leaching residue

3.4 Leaching kinetic analysis

Figure 10(a) presents the leaching rate of aluminum versus leaching time at different temperatures. Regarding that the shrinking unreacted core model (SCM) is widely used to illustrate the liquid-to-solid reaction [45−47], SCM was adopted herein to investigate the leaching kinetics of aluminum from alkali roasting residue at different leaching time (1−120 min) and temperatures (20−80 °C) under fixed leaching conditions of liquid/solid ratio of 8 and stirring speed of 300 r/min.

If the water leaching process of $NaAlO_2$ was controlled by chemical reaction, the equation of reaction rate could be described as Eq. (16). If the water leaching process of $NaAlO_2$ was controlled by the diffusion of the product layer, the equation of reaction rate could be described as Eq. (17):

$$1-(1-x)^{1/3}=kt \quad (16)$$

$$1-2/3x-(1-x)^{2/3}=kt \quad (17)$$

where k is the reaction rate constant; x is the leaching rate; t is the reaction time.

The data in Fig. 10(a) are plotted according to Eqs. (16) and (17). The plots of $1-(1-x)^{1/3}$ vs t at different temperatures are shown in Fig. 10(b) and the plots of $1-2/3x-(1-x)^{2/3}$ vs t are shown in Fig. 10(c). As displayed in Fig. 10(c), the correction coefficients R^2 of the linear fitting for the water leaching process of aluminum were high, confirming that the water leaching process of alkali roasting residue was well fitted with the diffusion control. The variation of leaching rate constant with temperature could be expressed by the Arrhenius equation (Eq. (18)). Figure 10(d) exhibits the natural logarithm of the reaction rate constant $\ln k$ as a function of the inverse temperature. According to Eq. (18), the apparent activation energy of water leaching was calculated to be 3.44 kJ/mol, which further verified that the water leaching process was subjected to the diffusion.

$$k=A_0\exp[-E_a/(RT)] \quad (18)$$

where A_0 is the pre-exponential factor; E_a is the apparent activation energy, kJ/mol; T is the reaction temperature, K; R is the molar gas constant, 8.314 J/(mol·K).

3.5 Mechanism of alkali roasting-leaching

The experimental results exhibited that the difficulty in increasing the conversion rate of sodium aluminate lay in the incomplete reaction of metallic aluminum which was caused by the fact that metallic aluminum had to be transformed into aluminum oxide before its reaction with sodium

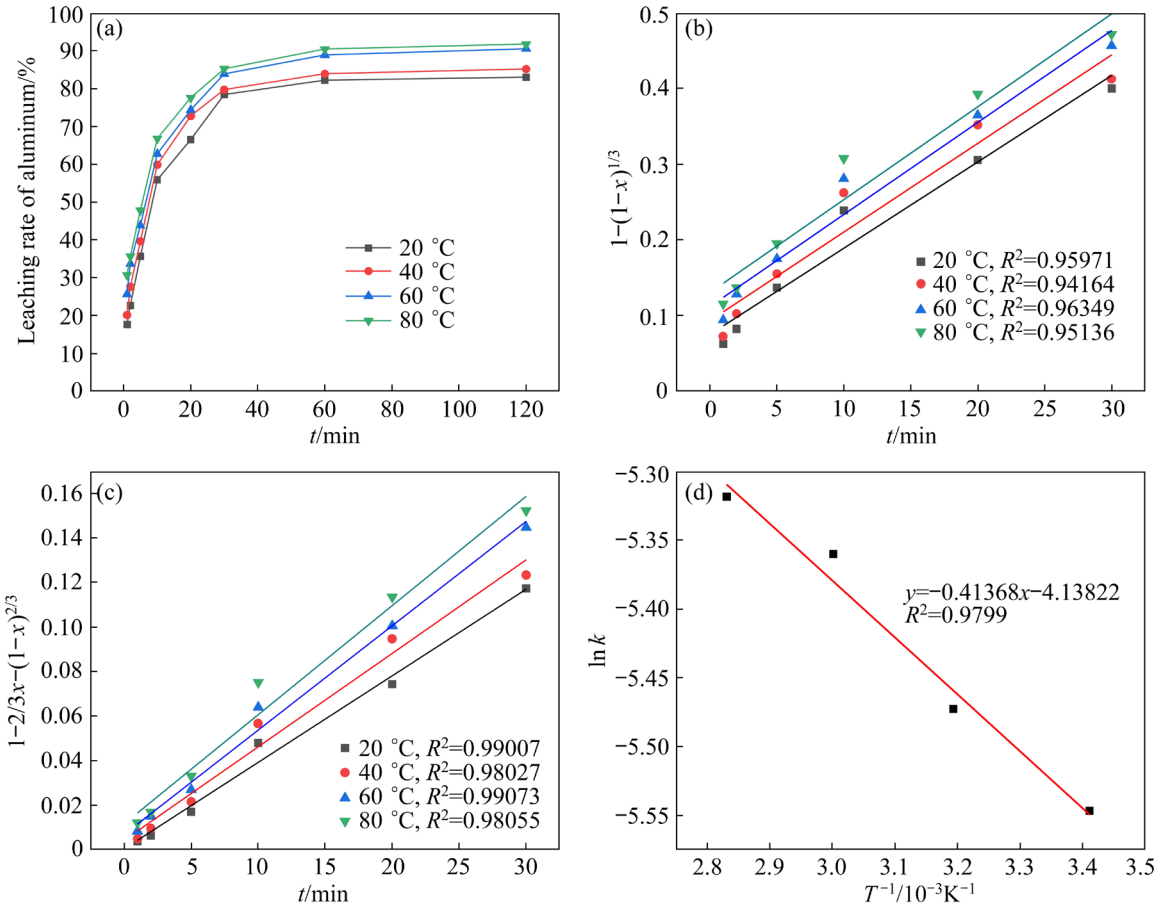

Fig. 10 Leaching results of aluminum (a), plots of $1-(1-x)^{1/3}$ (b) and $1-2/3x-(1-x)^{2/3}$ (c) vs leaching time t, and Arrhenius plot for dissolution of (d)

hydroxide. However, a dense aluminum oxide layer could form on the surface of metallic aluminum and hinder the oxidation reaction. Only after sodium hydroxide reacted with the aluminum oxide layer could the interior aluminum be further oxidized, thereby the generation of sodium aluminate was greatly limited. The reaction mechanism model of aluminum oxide and metallic aluminum in alkali roasting process is shown in Fig. 11. It can be seen that metallic aluminum, compared with aluminum oxide, was less prone to react with sodium hydroxide to generate $NaAlO_2$. In addition, it could be found from the water leaching experiment that the leaching rate of aluminum by water leaching was slightly higher than the conversion rate of $NaAlO_2$. This indicated that some unreacted metallic aluminum in the residue could be further dissolved to generate $NaAlO_2$ during the leaching process though the leaching rate was lower and longer reaction time was required. The reason for this phenomenon was similar to that of the roasting process. The dense aluminum oxide layer formed on the surface of metallic aluminum via oxidation during the water leaching process hindered the dissolution. Moreover, besides sodium meta-aluminate, it was seriously difficult for aluminum-containing phases to dissolve in the water leaching process.

4 Conclusions

(1) The alkali roasting process was an efficient treatment process for secondary aluminum dross with high content of metallic aluminum. In the alkali roasting process of secondary aluminum dross, the oxidation reaction of metallic aluminum was a key aspect to converting aluminum into $NaAlO_2$. Increasing the roasting temperature and the amount of alkali can promote the conversion of metallic aluminum. Under optimal roasting conditions, i.e., NaOH/SAD mass ratio of 1.0, roasting temperature of 800 °C, and roasting time of 1 h, 90.78% aluminum could be converted to $NaAlO_2$.

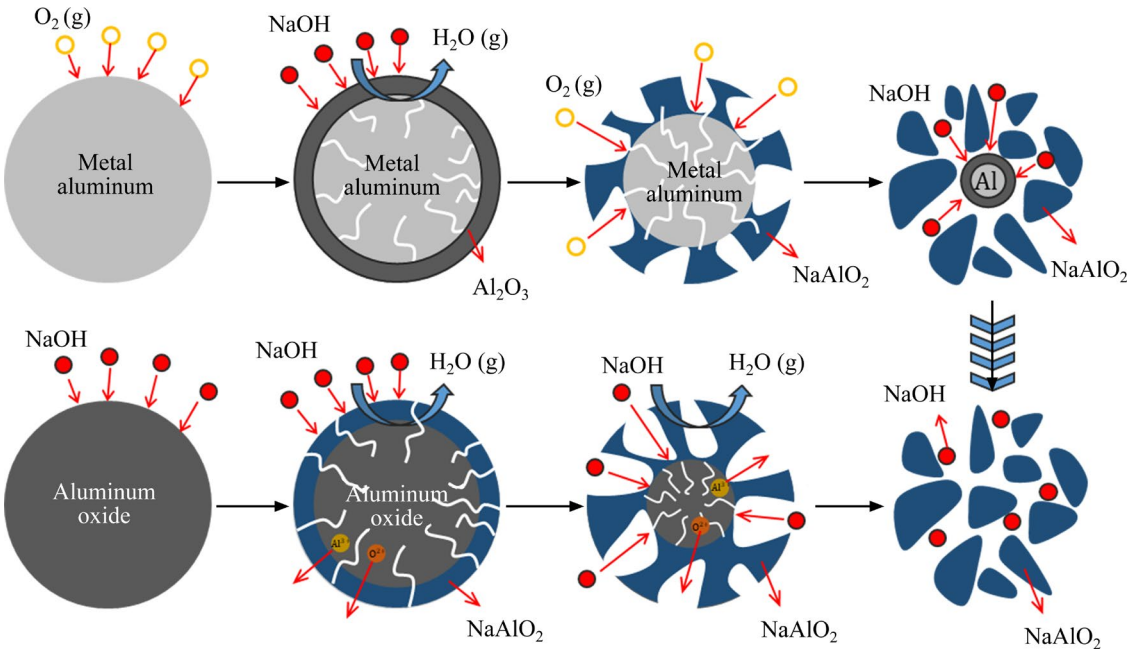

Fig. 11 Schematic diagram for mechanism of alkali roasting process of secondary aluminum dross

(2) The water leaching rate of aluminum in the roasted residue was closely related to the conversion rate of $NaAlO_2$. Increasing the leaching temperature and time were both conducive to the dissolution of other aluminum-containing phases. Under optimal water leaching conditions, i.e., leaching temperature of 80 °C, leaching time of 1 h and liquid/solid ratio of 8.0, 93.08% aluminum could be extracted.

(3) Kinetic study demonstrated that the water leaching process was in accord with the shrinking core model and the roasted residue dissolution was in accord with the diffusion control model, where the apparent activation energy was 3.44 kJ/mol.

CRediT authorship contribution statement

Chen LI: Methodology, Investigation, Writing − Original draft preparation; **Wei LIU:** Conceptualization, Methodology, Funding acquisition; **Fen JIAO:** Project administration, Funding acquisition; **Liang-min DONG:** Conceptualization, Investigation; **Shi-yang LIU:** Investigation, Methodology; **Wen-qing QIN:** Supervision, Funding acquisition.

Declaration of competing interest

The authors declare that they have no known competing financial interests or personal relationships that could have appeared to influence the work reported in this paper.

Acknowledgments

The authors gratefully acknowledge the financial support from the National Natural Science Foundation of China (Nos. 51804342, 51874356), the National Key R&D Program of China (Nos. 2019YFC1907301, 2020YFC1909203), and the Innovation Driven Project of Central South University, China (No. 2020CX038).

References

[1] ZHU Xing-han, YANG Jin-zhong, YANG Yu-fei, HUANG Qi-fei, LIU Tao. Pyrometallurgical process and multi-pollutant co-conversion for secondary aluminum dross: A review [J]. Journal of Materials Research and Technology, 2022, 21: 1196−1211.

[2] SRIVASTAVA A, MESHRAM A. On trending technologies of aluminium dross recycling: A review [J]. Process Safety and Environmental Protection, 2023, 171: 38−54.

[3] TSAKIRIDIS P E. Aluminium salt slag characterization and utilization—A review [J]. Journal of Hazardous Materials, 2012, 217: 1−10.

[4] YANG Qun, LI Qi, ZHANG Guo-fan, SHI Qing, FENG Hai-gang. Investigation of leaching kinetics of aluminum extraction from secondary aluminum dross with use of hydrochloric acid [J]. Hydrometallurgy, 2019, 187: 158−167.

[5] MAHINROOSTA M, ALLAHVERDI A. Hazardous aluminum dross characterization and recycling strategies: A critical review [J]. Journal of Environmental Management, 2018, 223: 452−468.

[6] GIL A, KORILI S A. Management and valorization of aluminum saline slags: Current status and future trends [J]. Chemical Engineering Journal, 2016, 289: 74−84.

[7] KUDYBA A, AKHTAR S, JOHANSEN I, SAFARIAN J.

Valorization of aluminum dross with copper via high temperature melting to produce Al−Cu alloys [J]. Materials, 2021, 14(15): 4117.

[8] ZHANG Yuan-bo, LIN Kun, SU Zi-jian, XU Jia-mei, JIANG Tao. Self-driven hydrolysis mechanism of secondary aluminum dross (SAD) in the hydrometallurgical process without any additives [J]. Chemical Engineering Journal, 2023, 466: 143141.

[9] SHEN Han-lin, LIU Bo, EKBERG C, ZHANG Shen-gen. Harmless disposal and resource utilization for secondary aluminum dross: A review [J]. Science of the Total Environment, 2021, 760: 143968.

[10] BRUCKARD W J, WOODCOCK J T. Characterisation and treatment of Australian salt cakes by aqueous leaching [J]. Minerals Engineering, 2007, 20: 1376−1390.

[11] DAVID E, KOPAC J. Hydrolysis of aluminum dross material to achieve zero hazardous waste [J]. Journal of Hazardous Materials, 2012, 209: 501−509.

[12] KUDYBA A, AKHTAR S, JOHANSEN I, SAFARIAN J. Aluminum recovery from white aluminum dross by a mechanically activated phase separation and remelting process [J]. JOM, 2021, 73: 2625−2634.

[13] SHINZATO M C, HYPOLITO R. Effect of disposal of aluminum recycling waste in soil and water bodies [J]. Environmental Earth Sciences, 2016, 75: 1−10.

[14] ZHU Xue-yuan, JIN Qiang, YE Zhen. Life cycle environmental and economic assessment of alumina recovery from secondary aluminum dross in China [J]. Journal of Cleaner Production, 2020, 277: 123291.

[15] HU K T, REED D, ROBSHAW T J, SMITH R M, OGDEN M D. Characterisation of aluminium black dross before and after stepwise salt-phase dissolution in non- aqueous solvents [J]. Journal of Hazardous Materials, 2021, 401: 123351.

[16] GAO Qin, GUO Qiang, LI Yong-li, REN Bao-zeng, FU Ming-bo, LI Hui-lin, TIAN Deng-chao, DING Min. Innovative technology for defluorination of secondary aluminum dross by alkali leaching [J]. Minerals Engineering, 2021, 172: 107134.

[17] SARKER M S R, ALAM M Z, QADIR M R, GAFUR M A, MONIRUZZAMAN M. Extraction and characterization of alumina nanopowders from aluminum dross by acid dissolution process [J]. International Journal of Minerals, Metallurgy, and Materials, 2015, 22: 429−436.

[18] DASH B, TRIPATHY B C, BHATTACHARYA I N, DAS S C, MISHRA C R, PANI B S. Effect of temperature and alumina/caustic ratio on precipitation of boehmite in synthetic sodium aluminate liquor [J]. Hydrometallurgy, 2007, 88: 121−126.

[19] AMER A M. Aluminum extraction from aluminum industrial wastes [J]. JOM, 2010, 62(5): 60−63.

[20] LOU Wen-bo, ZHANG Yang, ZHANG Ying, ZHENG Shi-li, SUN Pei, WANG Xiao-jian, LI Jian-zhong, QIAO Shan, ZHANG Yi, WENZEL M, WEIGAND J J. Leaching performance of Al-bearing spent $LiFePO_4$ cathode powder in H_2SO_4 aqueous solution [J]. Transactions of Nonferrous Metals Society of China, 2021, 31(3): 817−831.

[21] HOW L F, ISLAM A, JAAFAR M S, TAUFIQ-YAP Y H. Extraction and characterization of γ-alumina from waste aluminium dross [J]. Waste and Biomass Valorization, 2017, 8(2): 321−327.

[22] MESHRAM A, SINGH K K. Recovery of valuable products from hazardous aluminum dross: A review [J]. Resources, Conservation and Recycling, 2018, 130: 95−108.

[23] TSAKIRIDIS P E, OUSTADAKIS P, AGATZINI-LEONARDOU S. Aluminium recovery during black dross hydrothermal treatment [J]. Journal of Environmental Chemical Engineering, 2013, 1: 23−32.

[24] ZHANG Yong, GUO Zhao-hui, HAN Zi-yu, XIAO Xi-yuan, PENG Chi. Feasibility of aluminum recovery and $MgAl_2O_4$ spinel synthesis from secondary aluminum dross [J]. International Journal of Minerals, Metallurgy, and Materials, 2019, 26: 309−318.

[25] SHI Ming, LI Ying, SHI Jun-jie. Fabrication of periclase and magnesium aluminate spinel refractory from washed residue of secondary aluminum dross [J]. Ceramics International, 2022, 48: 7668−7676.

[26] ZHANG Yong, GUO Zhao-Hui, WANG Shuo, XIAO Xi-yuan, HAN Zi-yu, HUANG Bo, NIE Yun-Fei. Sintering fabrication of gehlenite/magnesia−alumina spinel composites by secondary aluminum dross [J]. The Chinese Journal of Nonferrous Metals, 2018, 28: 334−339. (in Chinese)

[27] YOSHIMURA H N, ABREU A P, MOLISANI A L, CAMARGO A C D, PORTELA J C S, NARITA N E. Evaluation of aluminum dross waste as raw material for refractories [J]. Ceramics International, 2008, 34: 581−591.

[28] YANG S F, WANG T M, SHIE Z Y J, JIANG S J, HWANG C S, TZENG C C. Fine Al_2O_3 powder produced by radio-frequency plasma from aluminum dross [J]. IEEE Transactions on Plasma Science, 2014, 42: 3751−3755.

[29] SARAVANAKUMAR R, RAMACHANDRAN K, LALY L G, ANANTHAPADMANABHAN P V, YUGESWARAN S. Plasma assisted synthesis of γ-alumina from waste aluminium dross [J]. Waste Management, 2018, 77: 565−575.

[30] DU Chang-ming, SHANG Chao, GONG Xiang-jie, WANG Ting, WEI Xian-ge. Plasma methods for metals recovery from metal-containing waste [J]. Waste Management, 2018, 77: 373−387.

[31] PARIRENYATWA S, ESCUDERO C L, SANCHEZ S S, HARA Y, JHA A. Comparative study of alkali roasting and leaching of chromite ores and titaniferous minerals [J]. Hydrometallurgy, 2016, 165: 213−226.

[32] LIU Hai-yang, XIANG Nan, SHEN Xiao-yi, ZHAI Yu-chun, HAN Chao. Decrease of material burden in a novel alkali-saving reduction treatment process of nickel slag based on NaOH roasting [J]. JOM, 2020, 72: 2686−2696.

[33] GUO Qiang, QU Jing-kui, QI Tao, WEI Guang-ye, HAN Bing-bing. Activation pretreatment of limonitic laterite ores by alkali-roasting method using sodium carbonate [J]. Minerals Engineering, 2011, 24: 825−832.

[34] SANCHEZ S S, MAKANYIRE T, ESCUDERO C L, HARA Y, JHA A. Reclamation of reactive metal oxides from complex minerals using alkali roasting and leaching—An improved approach to process engineering [J]. Green Chemistry, 2015, 17(4): 2059−2080.

[35] GUO Hong-wei, WANG Jun, ZHANG Xiu-xia, ZHENG Feng, LI Peng. Study on the extraction of aluminum from aluminum dross using alkali roasting and subsequent

synthesis of mesoporous γ-alumina [J]. Metallurgical and Materials Transactions B, 2018, 49: 2906−2916.

[36] VALEEV D, PANKRATOV D, SHOPPERT A, SOKOLOV A, KASIKOV A, MIKHAILOVA A, SALAZAR-CONCHA C, RODIONOV I. Mechanism and kinetics of iron extraction from high silica boehmite–kaolinite bauxite by hydrochloric acid leaching [J]. Transactions of Nonferrous Metals Society of China, 2021, 31(10): 3128−3149.

[37] XIE Bo-yi, LIU Cha-xiang, WEI Bo-han, WANG Rui-xiang, REN Ru-shan. Recovery of rare earth elements from waste phosphors via alkali fusion roasting and controlled potential reduction leaching [J]. Waste Management, 2023, 163: 43−51.

[38] DONG Zhong-lin, LI Qian, RAO Xue-fei, XU Bin, YANG Yong-bin, DONG Hai-gang, JIANG Tao. Economical and efficient recovery of Pd and Al_2O_3 from spent Pd/Al_2O_3 catalyst with integrated sodium roasting−reductive leaching process [J]. Transactions of Nonferrous Metals Society of China, 2023, 33(7): 2245−2254.

[39] LI Yong, QIN Zi-yi, LI Chun-lei, QU Yi, WANG Hai-bin, PENG Li, WANG Yi. Hazardous characteristics and transformation mechanism in hydrometallurgical disposing strategy of secondary aluminum dross [J]. Journal of Environmental Chemical Engineering, 2021, 9: 106470.

[40] ZUO Zheng-ping, LV Han, LI Rong-bin, LIU Feng-qin, ZHAO Hong-liang. A new approach to recover the valuable elements in black aluminum dross [J]. Resources, Conservation and Recycling, 2021, 174: 105768.

[41] THI T, LEE M S, THI H N. Ball milling treatment of black dross for selective dissolution of alumina in sodium hydroxide leaching [J]. Processes, 2018, 6(4): 29.

[42] VALEEV D, KUNILOVA I, SHOPPERT A, SALAZAR C C, KONDRATIEV A. High-pressure HCl leaching of coal ash to extract Al into a chloride solution with further use as a coagulant for water treatment [J]. Journal of Cleaner Production, 2020, 276: 123206.

[43] XIANG Jun-yi, WANG Xin, PEI Gui-shang, HUANG Qing-yun, LU Xue-wei. Recovery of vanadium from vanadium slag by composite roasting with CaO/MgO and leaching [J]. Transactions of Nonferrous Metals Society of China, 2020, 30(11): 3114−3123.

[44] SHEN Xiao-yi, HUANG Yan-xiang, SHAO Hong-mei, LIU Yan, GU Hui-min, ZHAI Yu-chun. Improvement of utilization efficiency of magnesite by $(NH_4)_2SO_4$ roasting–water leaching process [J]. Transactions of Nonferrous Metals Society of China, 2023, 33(2): 576−583.

[45] LV Han, XIE Ming-zhuang, SHI Li-tao, ZHAO Hong-liang, WU Ze-gang, LI Li-li, LI Rong-bin, LIU Feng-qin. A novel green process for the synthesis of high-whiteness and ultrafine aluminum hydroxide powder from secondary aluminum dross [J]. Ceramics International, 2022, 48: 953−962.

[46] WANG Hong-yang, ZHANG Xiao-xue, YANG Si-yuan, LIU Cheng, LUO Li-qun. Separation of alumina and silica from metakaolinite by reduction roasting−alkaline leaching process: Effect of $CaSO_4$ and CaO [J]. Transactions of Nonferrous Metals Society of China, 2022, 32(3): 999−1009.

[47] LV Han, ZHAO Hong-liang, ZUO Zheng-ping, LI Rong-bin, LIU Feng-qin. A thermodynamic and kinetic study of catalyzed hydrolysis of aluminum nitride in secondary aluminum dross [J]. Journal of Materials Research and Technology, 2020, 9: 9735−9745.

碱性焙烧–水浸工艺强化二次铝渣中金属铝的回收

李 琛，刘 维，焦 芬，董良民，刘世阳，覃文庆

中南大学 资源加工与生物工程学院，长沙 410083

摘　要：提出一种采用碱法焙烧−水浸强化回收二次铝渣中金属铝的创新工艺。利用热力学计算和实验结果阐明了碱焙烧过程的相变和反应机理，并对焙烧产物的浸出行为进行了研究。在最佳条件下，铝的提取率达到93.08%。此外，利用收缩核模型对焙烧产物的水浸动力学进行了研究，发现焙烧产物中铝的浸出过程受扩散控制；同时计算得到浸出过程的表观活化能为 3.44 kJ/mol。并且，在此基础上解释了二次铝渣碱性焙烧−水浸的反应机理。

关键词：二次铝渣；铝回收；选择性分离；碱性焙烧；水浸

(Edited by Wei-ping CHEN)